Molecular Human Reproduction, Vol.20, No.10 pp. 990–1001, 2014
Advanced Access publication on July 31, 2014 doi:10.1093/molehr/gau060

molecular human reproduction

ORIGINAL RESEARCH

NLRP7 inter-domain interactions: the NACHT-associated domain is the physical mediator for oligomeric assembly

Heike Singer[1], Arijit Biswas[1], Nicole Zimmer[1], Christiane Messaed[2,3], Johannes Oldenburg[1], Rima Slim[2,3], and Osman El-Maarri[1,*]

[1]Institute of Experimental Hematology and Transfusion Medicine, University of Bonn, Bonn, Germany [2]Department of Human Genetics, McGill University Health Centre Research Institute, Montreal, Canada [3]Department of Obstetrics and Gynecology, McGill University Health Centre Research Institute, Montreal, Canada

*Correspondence address. Institute of Experimental Hematology and Transfusion Medicine, University of Bonn, Sigmund-Freud-Str. 25, Bonn 53127, Germany. Tel: +49-228-287-16737; Fax: +49-228-287-14320; E-mail: osman.elmaarri@ukb.uni-bonn.de

Submitted on January 17, 2014; resubmitted on July 17, 2014; accepted on July 24, 2014

ABSTRACT: Mutations in *NLRP7* (NOD-like-receptor family, pyrin domain containing 7) are responsible for a type of recurrent pregnancy loss known as recurrent hydatidiform mole (HYDM1). This condition is characterized by abnormal growth of the placenta, a lack of proper embryonic development and abnormal methylation patterns at multiple imprinted loci in diploid biparental molar tissues. The role of NLRP7 protein in the disease manifestation is currently not clear. In order to better understand how the effects of HYDM1 are associated with mutations on the structure of NLRP7, we performed an inter-domain interaction screen using a yeast two-hybrid system. Additionally, we generated *in silico* structural models of NLRP7 in its non-activated and activated forms. Our observations from the yeast two-hybrid screen and modeling suggest that the NACHT-associated domain (NAD) of the NLRP7 protein is central to its oligomeric assembly. Upon activation, the NAD and a small part of the leucine rich repeat (LRR) of one molecule emerged out of the protective LRR domain and interact with the NACHT domain of the second molecule to form an oligomer. Furthermore, we investigated the molecular basis for the pathophysiological effect of four missense mutations, three HYDM1-causing and one rare non-synonymous variant, on the protein using confocal microscopy of transiently transfected NLRP7 in HEK293T cells and *in silico* structural analysis. We found that with the two clinically severe missense mutations, L398R and R693W, the normal molecule to molecule interaction was apparently affected thus decreasing their oligomerization potential while aggresome formation was increased; these changes could disturb the normal downstream functions of NLRP7 and therefore be a possible molecular effect underlying their pathophysiological impact.

Key words: NLRP7 / inter-domain-interactions / HYDM1-causing mutations / aggresome / protein misfolding

Introduction

NLRP7 is a protein belonging to one of the four major families of pattern recognition receptors termed nucleotide-binding oligomerization domain (Nod)-like receptors (NLRs). NLRs are a class of intracellular innate sensors for pathogen-associated molecular patterns (PAMPs) and damage-associated molecular patterns (DAMPs) sharing three functional domains: the N-terminal effector domain Pyrin (PYD) for downstream signaling, a central NACHT domain with its NACHT-associated domain (NAD) for oligomerization and a C-terminal leucine rich repeat (LRR) region for sensing PAMPs and DAMPs. The different NLR subfamilies are distinguished by their heterogeneous N-terminal effector domains, which could be either a pyrin domain (PYD), a baculovirus inhibitor of apoptosis domain (BIR) or a caspase activation and recruitment domain (CARD). NLRP7 belongs to the PYD containing NLR group (termed NLRP).

Like all NLRs, NLRP7 contains an NTPase domain that is characterized by two strongly conserved sequence motifs, Walker A/P-loop and Walker B, at the N-terminus of the NACHT domain. Because of these two motifs the NLRs belong to the clade of STANDs (Signal Transduction ATPases with Numerous Domains) within the AAA^{+} superfamily (ATPases associated with various cellular activities) (Leipe *et al.*, 2004). NTPases preferentially bind ATP or GTP on the Walker A/Ploop, while the free energy produced during NTP hydrolysis triggered

by the Walker B bound Mg^{2+} induce conformational changes in neighboring regions of the protein (Danot *et al.*, 2009). Several experiments testing nucleotide dependence on different STANDs (for instance with APAF1, NLRP1, NLRP3) developed an approved model of activation, which assumes the protein to switch between a non-active monomer and an activated NTP bound oligomer that forms a platform for downstream signaling adaptors of inflammasome (Duncan *et al.*, 2007; Faustin *et al.*, 2007; Reubold *et al.*, 2009).

Within the subfamily of NLRPs, NLRP1, NLRP3 and NLRP7 are known to serve as a sensor for PAMPs and DAMPs to form a multiprotein complex with ASC (apoptosis-associated speck-like protein containing a CARD) and caspase-1. Inflammasome activation is dependent on the specificity of NLRPs sensing their respective ligands. NLRP1 senses muramyl dipeptide and anthrax lethal toxin (Boyden and Dietrich, 2006; Faustin *et al.*, 2007). NLRP7 is known to oligomerize after activation by acylated lipopeptides (Khare *et al.*, 2012), while NLRP3 is also known to sense lipopolysaccharides, muramyl dipeptide or viral RNA. For NLRP3, these different PAMPS are believed to be required only for its transcriptional upregulation, while a second DAMP-specific signal like reactive oxygen species, endosomal rupture or changes in the potassium efflux are required for oligomerization and inflammasome formation of NLRP3 (Mariathasan *et al.*, 2006; Petrilli *et al.*, 2007; Allen *et al.*, 2009; Martinon *et al.*, 2009).

All three inflammasome-forming NLRPs recruit the adaptor protein, ASC, through a PYD-PYD specific interaction. ASC consists of an N-terminal PYD and a C-terminal CARD domain, which in turn recruits and activates caspase-1 through a CARD-CARD specific interaction (Carneiro *et al.*, 2008). The oligomerization of NLRPs is believed to connect the caspases, which leads to their activation and subsequent release of the inflammatory cytokines, interleukin-1β (IL-1β) and interleukin-18 (IL-18).

Apart from their role in the adaptive immune system, several NLRPs (NLRP2, NLRP5 and NLRP7) have a particular function in mouse and human reproduction. *NLRP5* was the first identified maternal effect gene (also known as MATER) where a knockout in mice blocks the development of the embryos at the 2-cell stage (Tong *et al.*, 2000). Similarly, a knock-down of *NLRP2* in mice leads to a complete developmental arrest at the 2-cell stage as well (Peng, 2012). In humans, in one family, a homozygous mutation in *NLRP2* was found in the mother of two offspring with the imprinting disorder Beckwith–Wiedemann syndrome (Meyer *et al.*, 2009). Apart from its developmental contribution, NLRP2 provides the same inflammatory functions as NLRP7 (Fontalba *et al.*, 2007). *NLRP7* is believed to have originated from a gene duplication event from *NLRP2*, which supports their equal contribution to both inflammation and development (Tian *et al.*, 2009).

Mutations in human *NLRP7* are associated with recurrent hydatidiform moles (HYDM1; MIM number: 60966) (Murdoch *et al.*, 2006). HYDM1 is an autosomal recessively inherited condition that leads to recurrent pregnancy loss characterized by excessive proliferation of the trophoblast, degeneration of chorionic villi and abnormal embryonic development. Homozygosity and compound heterozygosity have been described in HYDM1 patients (Messaed *et al.*, 2011b). *NLRP7* is located on the long arm of chromosome 19 (19q13.4) and to date ~42 different mutations have been reported in patients with two defective alleles (Slim and Wallace, 2013).

Apart from the classic phenotype of mole, the disease shows a high variability. Patients have been shown to suffer from other forms of reproductive loss, such as spontaneous abortions (SAs), stillbirths, malformed live births or even live births that have led to healthy adults (Nguyen and Slim, 2014). An additional screening of patients with only one molar pregnancy and at least three SAs discovered novel non-synonymous variants (NSVs) in NLRP7, all missenses in heterozygous state, indicating a milder phenotype for the disease with single heterozygous variants (Messaed *et al.*, 2011b).

As there is no mouse orthologue for *NLRP7*, analysis of its reproduction-related functions are much more complicated compared with other NLRPs. Most of the reported investigations are based on cellular models of either peripheral blood monocytes (PBMCs) from patients or transiently transfected HEK293T cells. DNA methylation analyses of molar tissues from patients with two NLRP7 mutations have shown abnormal methylation patterns on several imprinted regions (El-Maarri *et al.*, 2003; Kou *et al.*, 2008; Hayward *et al.*, 2009). While to date, it remains unclear as to how *NLRP7* mutations lead to a loss of DNA methylation at maternally imprinted loci, the fact that multiple imprinting control centers (ICs) are affected suggests an imprinting regulatory mechanism that works in trans (El-Maarri and Slim, 2006; Dias and Maher, 2013). Furthermore, a study with PBMCs from HYDM1 patients with different *NLRP7* mutations demonstrated a decreased secretion of IL-1β and TNF suggesting that an impaired cytokine secretion makes the patients tolerant to the growth of aberrant molar conceptions (Messaed *et al.*, 2011a).

To better understand the activation/oligomerization process of the NLRP7 protein and to study the possible pathophysiological effects of HYDM1-causing mutations on this process, we performed an intra-domain yeast two-hybrid screen. The potential interactions of the individual domains and deletion constructs suggest a crucial role for the NACHT-associated domain (NAD) as the mediator of oligomerization and for the LRR domain as an inhibitor of oligomerization, since all LRR-containing constructs, including the full-length wild-type NLRP7 protein, failed to reveal any interaction in the yeast system. The three HYDM1-causing missense mutations L398R, R693P, R693W and one NSV K511R in *NLRP7*, which we investigated, showed no effect in the yeast system. In contrast to the yeast system, the molecule to molecule interaction in HEK293T cells was clearly visible for the full-length wild-type NLRP7, the mutation R693P and the NSV K511R, while very faint for the two severe mutations, L398R and R693W. Also, in order to gain a structural perspective, we modeled NLRP7 on the crystal structure of murine APAF1, a protein with a similar domain architecture (Proell *et al.*, 2008). Since APAF1 performs its cellular function by the formation of an apoptosome, a heptameric oligomer resulting from the activation of APAF1, we also generated the model for activated NLRP7 based on a single particle electron density structure of the apoptosome. NLRP7 has also been previously shown to form oligomeric inflammasomes (Khare *et al.*, 2012). Therefore, with our model we were able to suggest putative structural changes that might occur during the activation/oligomerization process of NLRP7. This model confirmed the strong interaction potential of the NAD domain observed in our yeast two-hybrid studies. Finally with the help of these models and the confocal microscopy-based investigations of wild-type and mutated NLRP7, we suggest a molecular mechanism underlying the pathophysiological effect of the three investigated HYDM1-causing missense mutations and the one NSV, which is centered on the balance between normal oligomerization and aggregation.

Materials and Methods

Cloning DNA constructs

The yeast two-hybrid analysis was performed with full-length cDNA from human wild-type NLRP7, the individual NLRP7 domains (PYD, NACHT, NAD, LRR) and five NLRP7 deletions constructs (ΔNAD/LRR, ΔLRR, ΔPYD/LRR, ΔPYD, ΔNACHT) (Fig. 1A), all of which were cloned by the Gateway system (Invitrogen). NLRP7 wild-type and the deletion constructs NAD and ΔLRR were provided in a Flag-specific vector (pcDNA3.1 (+)-Flag) and have been reported previously (Messaed *et al.*, 2011a). Yeast-expression vectors pGBKT7 and pGADT7 (Matchmaker Gal4 two-hybrid system) were converted to the Gateway system by introducing the Gateway-cassette reading-frame B: pGBKT7-G and pGADT7-G. After incorporating all cDNAs into pDONR201 entry vector, all constructs were transferred to the yeast expression vectors pGBKT7-G and pGADT7-G as fusion to the Gal4 DNA binding (DNA-BD) and activation domain (DNA-AD), respectively. Immunoprecipitation was done with N-terminal Flag-tagged and C-terminal Myc-tagged pcDNA3.1 vector into which the constructs NLRP7wt, NAD and ΔLRR were amplified with Flag- and Myc-vector specific PCR-primers (Supplementary data, Table S1) and inserted by restriction-free cloning using Phusion High Fidelity DNA Polymerase (Finnzymes/Thermo Scientific), respectively. Confocal microscopy investigations were performed using fluorescent vector pEGFP-C1 (Clontech) into which full-length NLRP7 was inserted by restriction-free cloning (Supplementary data, Table S1). The integrity of all clones was confirmed by direct sequencing of the whole insert.

Site-directed mutagenesis

NLRP7 missense mutations L398R, R693P and R693W and K511R were introduced into the full-length construct by site-directed mutagenesis (Supplementary data, Table SI) using *Pfu* Turbo DNA Polymerase (Agilent Technologies). The integrity of all clones was confirmed by direct sequencing of the whole insert.

Yeast two-hybrid

Yeast two-hybrid analysis was performed with the Matchmaker GAL4 two-hybrid System (Clontech). Human cDNA of all 10 *NLRP7* constructs were fused to GAL4 DNA-BD (pGBKT7 vector) and screened against Gal4 DNA-AD (pGADT7 vector) *NLRP7* fusion constructs to conduct yeast transformations in an 'each against all' approach consisting of in total 100 independent combinations. The plasmids were introduced into the yeast strain AH109 by the recommended small-scale lithium acetate method. Positive double transformants were plated on selective dropout medium -Trp/-Leu (Clontech). Two to three colonies of positive double transformants were suspended in sterile water, replated on selective dropout media -Trp/-Leu/-His 'SDmed' and -Trp/-Leu/-His/-Ade 'SDhigh' (Clontech) and tested for interactions. All interactions that appeared in a double symmetric manner were considered as double positive.

Co-immunoprecipitation

HEK293T cells were cultured according to the recommended protocol and co-transfected (using Lipofectamine 2000; Invitrogen) with 2 μg of an appropriate Myc- and/or Flag-tagged expression plasmid. After 48 h of transfection, cells were washed twice with PBS (PAA), harvested and incubated in RIPA buffer (Sigma) for 20 min at 4°C. For each immunoprecipitation 40 μl of anti-Flag M2 affinity gel (Sigma) was washed twice with PBS. Subsequently 0.2 ml of cell lysates was added and incubated overnight at 4°C. Agarose beads were washed extensively 5–6 times with PBS prior to eluting the coupled proteins by incubating in 30 μl of 2× Laemmli buffer (Bio-Rad) with 5% β-Mercaptoethanol, which were then resolved on a 10% SDS-polyacrylamide gel (TGX Precast Gels, Bio-rad). Resolved proteins were transferred to PVDF membranes (Whatman Westran PVDF membrane, Sigma). Immunoblotting for Myc-tagged constructs was carried out using anti-c-Myc-HRP at 1:2500 (Miltenyi Biotec) or anti-c-Myc at 1:500 (Sigma) followed by anti-rabbit horseradish peroxidase-conjugated secondary antibody (1:4000). Chemiluminescence was detected by a luminol/HRP reaction solution (1 ml solution A [0.1 M Tris–HCL, 25 mg luminol] + 100 μl solution B [11 mg 4-hydroxycoumarin, 10 ml DMSO] + 1.3 μl hydrogen peroxide). Immunoblotted Flag-tagged constructs were incubated with anti-Flag-M2-AP at 1:1000 and detected with CDP-Star (both from Sigma).

Confocal microscopy and immunostaining

HEK293T cells were placed on glass coverslips before co-transfection with 400 ng of EGFP-tagged expression plasmid. After 24 h, cells were washed twice with PBS and fixed in 4% PFA for 5 min. Cells were blocked with PBS containing 10% FBS and 0.1% Triton for 15 min and then incubated with each of the primary antibodies: anti-γ-tubulin (1:100) (sc-17788, Santa Cruz), anti-ubiquitin (1:100) (sc-271289, Santa Cruz), anti-26s-proteasome (1:100) (ab58115, abcam) or anti-vimentin (1:100) (sc-5565, Santa Cruz) overnight at 4°C, followed by incubation with the appropriate secondary antibody Alexa Fluor 555-conjugated Donkey anti-Mouse (1:1000) (A31570, Invitrogen) or Alexa Fluor 555-conjugated Goat anti-Rabbit (1:1000) (A21428, Invitrogen). Nuclei were stained using To-Pro-3 (T3605, Invitrogen). After three more washing steps with PBS, the cells were mounted with Vectashield mounting medium (Vector Laboratories) and examined with an Olympus Fluoview FV 1000 confocal microscope (Olympus).

Modeling of non-activated and activated NLRP7

Domain annotation of the NLRP7 protein was done using a combination of different servers [Domaination http://www.ibi.vu.nl/programs/domainationwww/, PrDos http://prdos.hgc.jp/cgi-bin/top.cgi (Ishida and Kinoshita, 2007), Supplementary data, Fig. S1A and B]. Once domain boundaries and connecting linkers were determined, we proceeded with the modeling of the non-activated and activated NLRP7 protein. Modeling of the NLRP7 protein was done on the ITASSER server (http://zhanglab.ccmb.med.umich.edu/I-TASSER/) using user specified constraints/modeling option-1 (Zhang, 2008). The crystal structure of murine APAF1 (PDB ID: 3SFZ) at 3 Å resolution was submitted as the user specified constraint for the non-activated NLRP7 structure and a single particle, electron density map-based structure of an APAF1 apoptosome (PDB ID: 3J2T) of ~9.5 Å resolution was used as the user specified constraint file for the activated NLRP7 (Zhang, 2008). Additionally each domain apart from the PYD domain [for which there is a crystal structure; PDB ID: 3SFZ (Pinheiro *et al.*, 2010)], was individually modeled using default settings on ITASSER. This was done on the assumption that there would be much more inter-domain than intra-domain movement during the process of activation as had earlier been shown for the homology-based model of NLRP3, which was also designed on the APAF1 structure (Proell *et al.*, 2008). The individually generated models and the crystal structure of the PYD domain were then replaced on the backbone of the completely modeled NLRP7 structure. Both, the non-activated and the activated structure were energy minimized through steps of local steepest descent minimization without electrostatics to remove bumps and simulated annealing minimization. Both structures were further refined running a short solvated refinement simulation lasting 500 ps. The structure from the trajectory with the lowest energy was chosen as the final structure. Stereochemical parameter qualities of the model and template structures were assessed and compared using the MOLPROBITY server (Davis *et al.*, 2007).

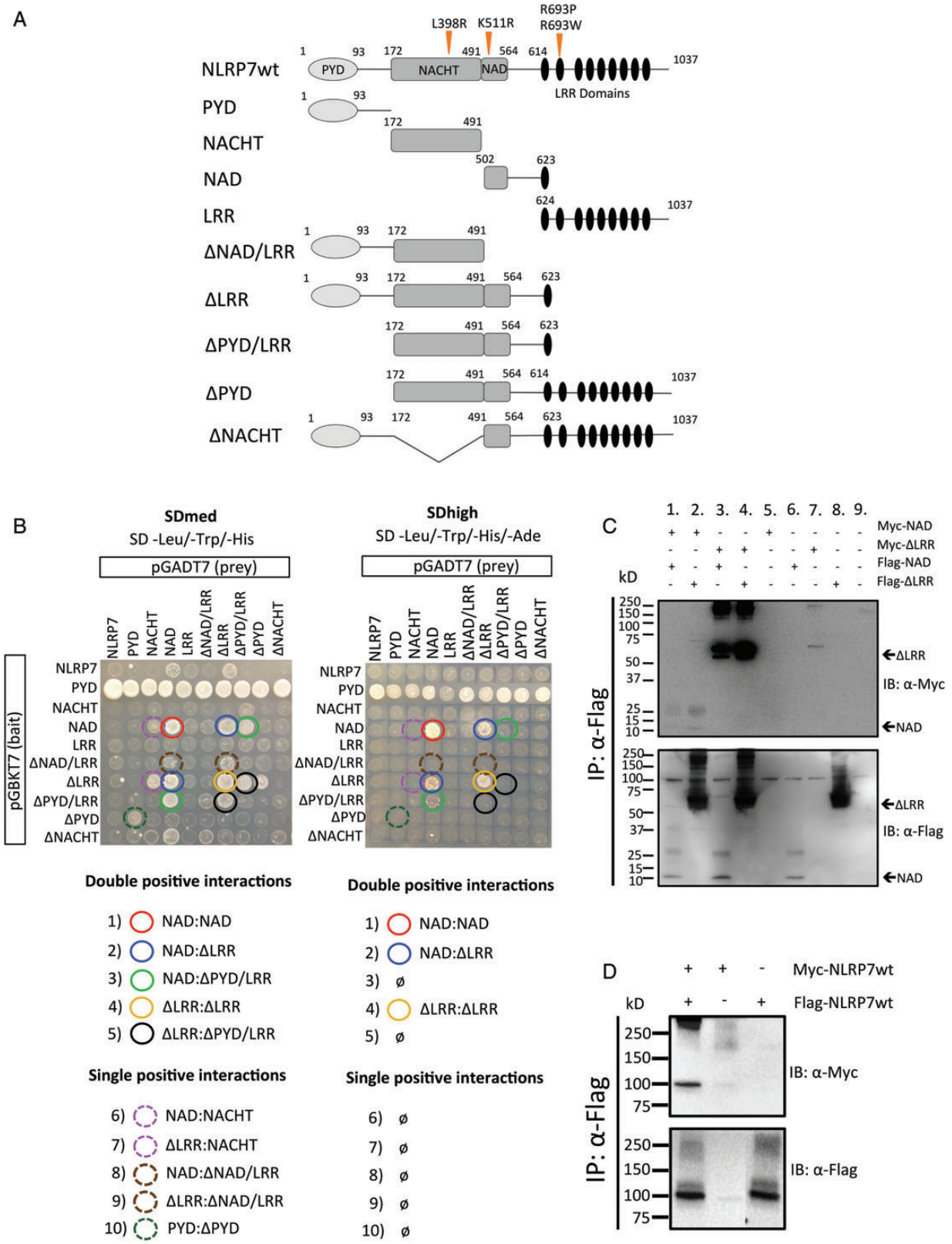

The final activated NLRP7 model was used as the input file for symmetric multimer docking on the M-ZDock server (http://zdock.umassmed.edu/m-zdock/) (Davis *et al.*, 2007). Considering similar sizes for APAF1 (1248 amino acids) and NLRP7 (1037 amino acids), a symmetry count of $n = 7$, which is also observed in the single particle, the electron density-based structure of APAF1 (PDB ID: 3J2T) was submitted as a criterion (Yuan *et al.*, 2013). In order to understand the structural consequences of the chosen missense mutations (reported in patients with recurrent hydatidiform moles) in our study, we assessed the local molecular environment corresponding to these mutations and their likely biophysical impact on the protein. Structural analysis, visualization and image rendering were done with the YASARA version and the Chimera version (Krieger *et al.*, 2002; Pettersen *et al.*, 2004). Additionally the impact was assessed by performing *in silico* mutagenesis for these mutations on the modeled non-activated NLRP7 structure using the SWAP function of YASARA followed by optimization for the mutated residue by choosing the best possible rotamer. The local environment of the mutated residue post *in silico* mutagenesis was compared with the wild-type residue. Separate free energy calculations were also made for each mutation using the FOLD-X plug-in embedded in the YASARA version (Van Durme *et al.*, 2011) in order to access its impact on the folding of protein. The non-activated structure was also submitted to the COACH protein-ligand binding site prediction meta-server (http://zhanglab.ccmb.med.umich.edu/COACH/) (Yang *et al.*, 2013).

Results

NLRP7 inter-domain interactions: a yeast two-hybrid analysis

The extensive analysis of our inter-domain interactions revealed clear identification of domains that drive dimerization and ultimately oligomerization of the molecules. The most obvious interaction was mediated by the NAD–NAD interaction and the most obvious interaction-inhibitor was the presence of the LRR. Thus the key characteristic of an interacting molecule was the presence of an NAD domain and the absence of an LRR domain (Fig. 1B).

However, we also observed an exception to the above rule, whereby single domain interactions involved domains, such as the NACHT with both, the single NAD and a vector lacking the LRR (Fig. 1B, left panel). Furthermore, the PYD domain presented a single interaction with a PYD deleted molecule, apart from the false positive yeast activation of the PYD fused to the BD. These additional interactions were only observed on the less stringent medium SDmed and only with one vector combination and not after vector switch. This could be due to the relatively weak/unstable interaction and/or to the different effects of fused AD or BD vector protein domains on the configurations of the attached NLRP7 domains.

All three interactions from the high stringency medium were verified by co-immunoprecipitation (Fig. 1C). Therefore, the NLRP7 cDNA constructs of both Myc- and Flag-tagged NAD and ΔLRR were co-transfected in all four possible combinations into HEK293T cells. Immunoprecipitation was performed using anti-Flag antibody. The NAD domain (13 kDa) and the ΔLRR deletion construct (68 kDa) were co-precipitated by self-protein and by each other (Fig. 1C). Although the expression of the NAD domain in HEK293T cells turned out to be quite weak, the precipitated NAD monomer (IB α-Flag) as well as the co-precipitated NAD monomer (IB α-Myc) were clearly visible at a size of 13 kDa after immunoblotting with anti-Flag and anti-Myc, respectively. Furthermore, NAD co-precipitated with ΔLRR and ΔLRR co-precipitated with NAD and ΔLRR. In contrast to the yeast system, immunoprecipitation of full-length NLRP7 (113 kDa) showed a positive interaction with the self-protein, most probably due to the presence of a proportion of the activated state in HEK293T or to the absence of GAL4 fusion proteins present in the yeast system which could hinder the interaction of the full molecule (Fig. 1D).

An APAF1 based model for NLRP7 activation and oligomerization

Independent of the yeast analysis, a model of the activated and the non-activated NLRP7 protein was generated, based on homology to APAF1, to elaborate potential structural rearrangements during activation. The activated as well as the non-activated models of NLRP7 showed distinct demarcations into PYD, NACHT, NAD and LRR domains (Fig. 2A). Additionally, two differences between active and inactive forms were noticed. First, the NAD domain, which is deeply entrenched in the LRR domain of the non-activated NLRP7, was observed to be free from any such sequestration in the activated structure, suggesting most likely that this domain participates in oligomerization after activation. Second, in the activated form bending of the PYD and NACHT

Figure 1 Inter-domain interactions of NLRP7. (**A**) Diagram of the 10 different NLRP7 constructs used for yeast two-hybrid screen marked with the mutations and variant (orange arrowheads) analyzed in this study. NLRP7 consists of four functional domains, PYD (light gray), NACHT and the NAD (gray) and LRR domain (black). Amino acid numbering in each construct is shown above. (**B**) Yeast two-hybrid screen performed with the Gal4-System (Clontech). A total number of 100 (10 × 10) NLRP7 construct combinations was analyzed in an 'each against all' screen. Inter-domain interactions (marked with colored circles) are presented on selective dropout medium 'SDmed' lacking three amino acids (left panel) and on 'SDhigh' lacking four amino acids (right panel). SDmed observed five double positive interactions: (1) NAD:NAD (red); (2) NAD:ΔLRR (blue); (3) NAD:ΔPYD/LRR (green); (4) ΔLRR:ΔLRR (yellow); (5) ΔLRR:ΔPYD/LRR (black); and five single positive interactions: (6) NAD:NACHT and (7) ΔLRR:NACHT (dashed violet); (8) NAD:ΔNAD/LRR and (9) ΔLRR:ΔNAD/LRR (dashed brown). PYD as bait (pGBKT7) induced false positive interaction with all 10 NLRP7 constructs as prey (pGADT7), while PYD as prey (pGADT7) shows a single interaction with ΔPYD: (10) PYD:ΔPYD (dashed dark-green). On SDhigh, only the strong interactions between NAD and ΔLRR remained (1), (2) and (4) (red, blue and yellow), while all other interactions disappeared. (**C**) Verification of inter-domain interactions by Flag-immunoprecipitation in HEK293T cells. Immunoblots (IB) were probed with Flag-specific (lower panel) and Myc-specific antibody (upper panel). N-terminal Flag-tagged NAD (13 kDa) and ΔLRR (68 kDa) in the lower panel, co-precipitated with C-terminal Myc-tagged self-protein or with each other. Both, the NAD domain and ΔLRR show an additional more diffuse band around 26 kDa and between 150–250 kDa, respectively, indicating additional aggregate/oligomer formation triggered by the prior heat treatment for SDS–PAGE. (**D**) Co-immunoprecipitation of Myc-tagged NLRP7 with Flag-tagged self-protein in HEK293T cells (left side). Single immunoprecipitation of Flag-tagged NLRP7 and Myc-tagged NLRP7 as control (right side).

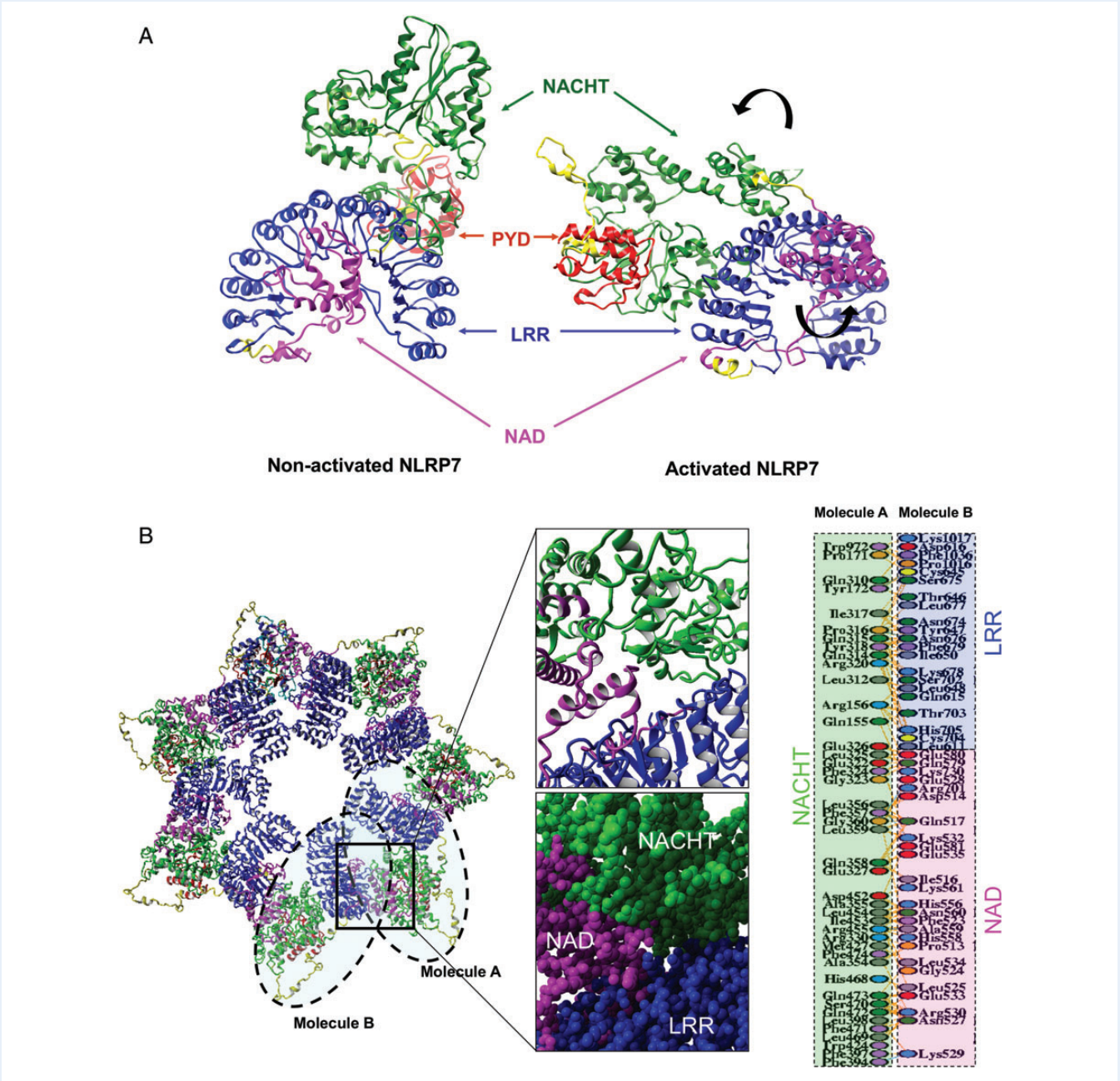

Figure 2 Activation and oligomerization of NLRP7. (**A**) The structural models of NLRP7 and its activated form in ribbon format. The individual domains are colored as follows: PYD domain (red), NACHT domain (green), NAD domain (magenta) and the LRR domain (dark blue). The yellow regions represent the linkers between these domains. (**B**) Heptagonal model of the inflammasome in ribbon form generated by symmetric multimeric docking of the monomeric activated model of NLRP7 on the Z-Dock multimer-docking server (MZ-Dock).

domains with respect to the whole protein exposed regions previously buried inside (Fig. 2A, right side).

The multimeric docking of the activated NLRP7 suggested major contacts between the NAD domain and a small part of the LRR of one molecule with the NACHT domain of a second molecule (Fig. 2B). The non-activated structure showed the NACHT domain specific binding site for ADP and Mg^{2+} ions on the COACH meta-server (Supplementary data, Fig. S3) where the binding site predictions included the conserved Walker A and Walker B motifs previously described in the literature for the NLRP group of proteins (Yang *et al.*, 2013). The main intra-domain structural changes observed in the activated structure (and therefore during activation) were near these motifs (and hence in the NACHT domain, Fig. 2A), further emphasizing the importance of these motifs for ligand binding and subsequent oligomerization. The NAD domain, apart from moving out of the LRR pocket in the activated structure, also showed a characteristic exposure of some hydrophobic residues to the surface, which was not as evident in the non-activated structure, further supporting the possibility that this domain may be

the key participant in any oligomeric assembly/aggregation (Supplementary data, Fig. S4).

Mutations responsible for HYDM1 do not change the interaction phenotype of full-length NLRP7 in the yeast two-hybrid system but negatively affect co-immunoprecipitation in HEK293T cells

To investigate the effect of reported mutations leading to HYDM1, we selected three missense mutations and one NSV from the Infevers database (http://fmf.igh.cnrs.fr/ISSAID/infevers/), containing hereditary auto-inflammatory disorders mutations. The three missense mutations were chosen because of the high severity of two (L398R and R693W) and the relatively lower severity of the third (R693P). L398R is located in the NACHT domain, while R693P and R693W are located in the LRR domain and represent a mutation hotspot (Fig. 1A). For the NAD domain, only nonsense or frameshift mutations are known. We therefore included the NAD-located rare NSV K511R based on the possible influence of this NSV in the genetic susceptibility to a milder phenotype of HYDM1.

To test whether the analyzed mutations influence the intra-domain interactions of NLRP7, we performed additional yeast two-hybrid screenings (Supplementary data, Fig. S2). Bait and prey constructs from wild-type NLRP7, the four mutated full-length *NLRP7* constructs, the single NAD domain and the ΔLRR deletion construct were tested in an 'each against all' approach for self- and non-self-interactions. Again, only the three already detected intra-domain interactions were found, while all other combinations remained negative suggesting that the analyzed HYDM1-linked mutations do not change the ability of the LRR domain to protect the highly reactive/hydrophobic NAD in the yeast two-hybrid system.

For the subsequent analyses by co-immunoprecipitation, we introduced the mutations into Flag- and Myc-tagged NLRP7 constructs. The wild-type and all four mutated NLRP7 constructs (all Flag-tagged) were co-transfected with Myc-tagged self-protein into HEK293T cells and precipitated with an anti-Flag antibody (Fig. 3A).

The less severe missense mutation R693P and the NSV K511R showed the same strong interaction with self-protein as the wild-type protein, while the severe missense mutations L398R and R693W co-precipitated very weakly with self-protein indicating much reduced dimer formations.

In silico mutagenesis of the analyzed HYDM1-causing mutations/variant

To investigate how the mutations influence the protein structure, we performed specific *in silico* mutagenesis for each of the four tested mutations.

The three HYDM1-causing missense mutations and the NSV showed differences in biochemical/biophysical aspects with respect to the wild-type residue when their local environment was inspected (Fig. 3B). The mutation at L398R presented an arginine residue partly exposed to the surface of the NACHT domain instead of the original fully exposed hydrophobic leucine residue. The NSV K511R on the NAD domain lead to a higher number of side-chain interactions (H-bonds and salt bridges) for the mutated arginine residue than those observed with the wild-type lysine residue. Most of the side-chain interactions were with residues from the LRR domain. The mutations R693P and R693W in the LRR domain both lead to non-conservative replacements of the same arginine residue to a surface-exposed hydrophobic tryptophan residue and a lesser hydrophobic proline residue, which will effectively break the helix on which the wild-type R693 originally sits. Free energy calculations [differences in the calculated free energies (ΔΔG) between the final state, 'the mutant', and the reference state, 'the wild-type protein'] for all mutations showed a negative impact (destabilizing mutations; the higher the ΔΔG values, the more the destabilizing effect) on folding with the highest, corresponding to the R693P, and the lowest, corresponding to R693W (free energy calculations: R693P = 2.78; K511R = 2.75; L398R = 2.29; R693W = 1.72).

Perinuclear accumulation of transiently transfected NLRP7 indicates an aggresome formation in HEK293T cells

In our confocal microscopy studies, overexpression of EGFP-NLRP7wt revealed, in some cells, a diffuse distribution in the cytoplasm and, in other cells, increased accumulations near the nucleus. The cell has different strategies to control the accumulation of misfolded cytosolic or aggregated proteins. Four different compartments are known to protect the cell from damaged and aggregated proteins, namely the juxtanuclear quality control (JUNQ), the insoluble protein deposit (IPOD), the endoplasmic reticulum-associated compartment (ERAC) and the aggresome (Bagola and Sommer, 2008). The IPOD, for example, harbors non-ubiquitylated proteins and is located apart from the nucleus. JUNQ, ERAC and the aggresome are found nearby the nucleus: they contain ubiquitylated polypeptides and are associated with proteasomes. The aggresome, in particular, is dependent on the microtubule organizing center (MTOC) and is surrounded by the intermediate filament protein vimentin (Johnston *et al.*, 1998). To identify the nature of the accumulation and possible aggregation in the cells, we investigated the co-localization of NLRP7 using potential aggresome markers, such as MTOC (anti-γ-tubulin), ubiquitin (anti-ub), the 26s proteasome (anti-26s proteasome) and vimentin (anti-vimentin) by immunofluorescence in HEK293T (Supplementary data, Fig. S6). As shown for the endogenous NLRP7 (Messaed *et al.*, 2011a), the juxtanuclear accumulation of transiently transfected NLRP7 showed a clear co-localization with the MTOC (Supplementary data, Fig. S6A–C). Furthermore our confocal studies revealed a co-localization with both ubiquitin and the 26s proteasome and therefore excluded the formation of an IPOD (Supplementary data, Fig. S6D–I). The proteasome is a molecular complex that controls intracellular protein homeostasis by degrading misfolded or regulatory proteins. The 26s proteasome is responsible for ATP-dependent degradation of polyubiquitinated proteins.

Finally, immunostaining with anti-vimentin demonstrated a sharp surrounding and co-localization of vimentin with the juxtanuclear accumulation and identified an NLRP7 aggresome (Supplementary data, Fig. S6J–L).

The amount of aggresome formation in HEK293T cells varied between different HYDM1-causing NLRP7 mutations

With the knowledge that the wild-type NLRP7 protein shows localization in the aggresome, we wanted to examine the effect of HYDM1-causing mutations on the localization of the protein within the cells. To

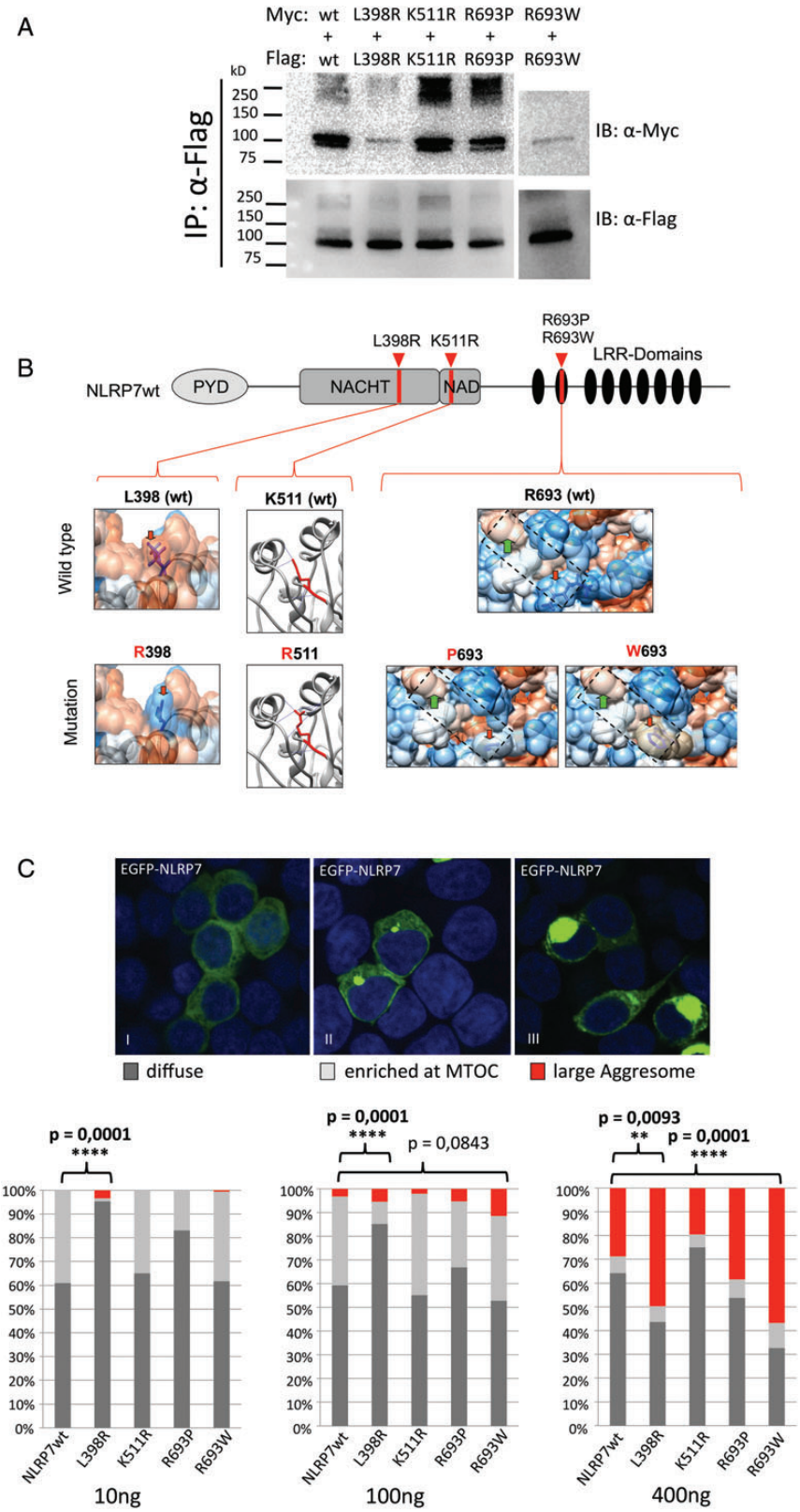

investigate whether the tested mutations influence the cellular localization, EGFP-tagged full-length protein was mutagenized for each of the four selected HYDM1-linked mutations/variant L398R, R693P, R693W and K511R. After transient transfection of 10, 100 and 400 ng into HEK293T cells, each construct was analyzed by confocal microscopy (Fig. 3C).

Compared with NLRP7wt, the NACHT-domain-associated mutation L398R and the LRR-domain-associated mutation R693W, clearly showed a high tendency of juxtanuclear aggregate formation at the three tested concentrations. After counting ~1000 cells in each experiment per construct (data not shown), cells were empirically grouped into three types of cells detected: diffusely distributed, enriched at MTOC and large aggresome (Fig. 3C, upper panel).

At 400 ng, the NLRP7 wild-type construct showed around 30% of cells with large aggresome formations in all three independent transfection reactions (Fig. 3C, lower panel), while for the missense mutation L398R (NACHT-domain), the amount of cells with a large aggresome increased to 50–54% (χ^2-test; $P = 0.0093$). Equally R693W showed large aggresome formations in 54% of cells ($P = 0.0001$).

Transfections with 10 and 100 ng revealed again the same tendency with higher aggresome formations for L398R and the R693W, albeit with a much lower percentages (Fig. 3C, lower panel). At a concentration of 100 ng, the mutation R693W was at the border of significance, while L398R showed, for 10 ng as well as 100 ng, a significant increase in cells with a diffuse protein distribution and an increase in cells with a large aggresome [L398R (10 ng): $P = 0.0001$, L398R (100 ng): $P = 0.0001$].

Discussion

In this study, we investigated the inter-domain interactions of NLRP7 by a yeast two-hybrid screen and identified (i) the NACHT domain as an activator for oligomerization (by virtue of its NTP binding domains), (ii) the NAD domain as the physical mediator for oligomerization due to its highly interactive potential and because of its interaction with the NACHT domain and (iii) the LRR domain as inhibitor of the highly reactive NAD domain due to the absence of inter-molecular interaction in its presence in the yeast system and because of its protection/engulfing of the NAD domain in the inactive state as predicted by the *in silico* modeling. Indeed, modeling of NLRP7 on the crystal structure of the APAF1 protein, which has a similar domain architecture as NLRP7, suggests putative structural changes that might occur during the activation/oligomerization process of NLRP7. Furthermore, confocal microscopy-based investigations of transiently transfected wild-type or mutated NLRP7 in HEK293T cells revealed varying amounts (but mutation specific) of aggresome formation within the cytoplasm, which may be caused by the inability to lead normal inter-molecular interactions.

Analysis of active and inactive state points to the NAD domain as the primary domain responsible for oligomeric assembly

In the non-activated NLRP7 model, the N-terminal PYD domain lies close to the LRR domain. After activation, the NACHT domain implements major structural rearrangements. Thus, the PYD domain faces outwards and is free for downstream signaling events (e.g. interaction with ASC). However, the NAD domain in the non-activated NLRP7 model lies completely in the hydrophobic inner pocket of the LRR domain and this explains the sequestering effect of the LRR domain, which while present, does not allow the NAD domain to interact with any other domain(s) (as observed in yeast). Additionally, a heptagonal symmetrical inflammasome model identified the NAD domain as the main interaction domain, which after activation moves outside of the LRR domain hydrophobic pocket and interacts during oligomerization with the NACHT of a second molecule.

The importance of NAD in mediating oligomerization is reinforced by two facts. First: when plotting the surface hydrophobicity on a Kyte & Doolittle scale, it becomes apparent that, in the activated state, an increasing number of hydrophobic residues become surface-exposed in the NAD domain, which increases its interaction potential and accelerates the oligomeric aggregation/assembly (Supplementary data, Fig. S4). The yeast analyses detected such an interaction as a single interaction between NAD and NACHT and between ΔLRR (thus containing the NAD) and NACHT on SDmed (Fig. 1B, dashed violet circle). Second:

Figure 3 HYDM1-causing mutations can influence aggresome formation in HEK293T cells. (**A**) Co-immunoprecipitation of Myc-tagged wild-type and mutagenized NLRP7 constructs with Flag-tagged self-protein using an anti-Flag-specific antibody. Immunoblots (IB) were probed with Flag-specific (lower panel, FlagIP) and Myc-specific antibody (upper panel, Co-IP). (**B**) Modeled missense mutations in the NLRP7 protein. This figure is divided into three representative images presenting the local molecular environment of the mutated and the wild-type residue (marked with a red arrow). Images on the left side depict the L398R mutation. The structure is represented by its molecular surface. Coloring is based on the Kyte and Doolittle coloring scale with blue representing hydrophilicity and orange hydrophobicity. The Leu398 residue is part of a large hydrophobic patch represented by the large orange surface. The backbone structure is represented as a gray ribbon. The residues of interest are depicted in stick format. The Arg398 residue stands out as the blue hydrophilic surface patch on the overall red hydrophobic surface. The images in the middle represent the K511R variant. The backbone structure is represented as a gray ribbon. The specific residue is shown in stick format. The side-chain interactions (hydrogen bonds and salt bridges) with neighboring residues from the LRR domain are depicted as blue lines. The images on the right side depict the mutations R693W and R693P. The structures are represented by their molecular surface as described for the L398R mutation. The green arrow indicates the proximal region to residue 693 that interacts with the NACHT domain in the heptagonal oligomer. The Trp693 variant clearly shows an increase in hydrophobicity on the overall surface area. (**C**) Upper panel: confocal analysis of overexpressed EGFP-tagged NLRP7 revealed three different phenotypes of cellular distribution: (I) diffuse distribution in the cytoplasm, (II) enrichment of juxtanuclear aggregates at the MTOC or (III) large aggresome formations. Lower panel: scoring the three different cell-phenotypes within the HYDM1 causing mutations L398R, R693P, R693W and K511R after three independent transfections with 10, 100 and 400 ng. Compared with the wild-type construct, R693W and L398R show, for all three concentrations, an increase in cells with large aggresome formation (red). At 400 ng, the formation of a large aggresome in the cells are significant for both mutations [L398R (400 ng): $P = 0.0093$, R693W (400 ng): $P = 0.0001$]. At a concentration of 100 ng, the mutation R693W shows borderline significance [R693W (100 ng): $P = 0.0843$, labeled in black], while L398R shows for both, 10 and 100 ng, a significant increase in cells with a diffuse protein distribution and an increase in cells with a large aggresome [L398R (10 ng): $P = 0.0001$, L398R (100 ng): $P = 0.0001$].

NLRP7 is a protein with a number of regions predicted to be prone to aggregation (Supplementary data, Fig. S5). Among these regions, the complete NAD domain is in a region with the highest susceptibility to aggregation.

Therefore, on the basis of the yeast two-hybrid system and the models, we conclude that the NAD domain of NLRP7 is the most crucial domain for inter-domain interactions within the oligomeric assembly. The NLRP7-based heptagonal oligomeric model shows that the NAD domain and a small area of the LRR domain of one molecule interact largely with the NACHT domain of a second molecule. Especially, the area surrounding the conserved sequence motifs Walker A and Walker B within the NACHT domain (Supplementary data, Fig. S3) shows internal structural rearrangements during the activation process in order to evert the PYD domain and to accommodate the now non-sequestered NAD domain and part of the LRR domain (Fig. 2B).

Local environment of missense mutations on the modeled NLRP7 structure and potential activation and oligomerization

Free energy calculations performed on our model for the three mutations and the variant investigated in this study suggests an almost equal negative impact on folding (free energy calculations: R693P = 2.78; K511R = 2.75; L398R = 2.29; R693W = 1.72). This is not surprising since all of these mutations, except K511R, are non-conservative in nature. The mutation R693W showed the lowest impact.

The first of these mutations, the L398R mutation in the NACHT domain, occurs on a residue that is part of a large surface-exposed hydrophobic patch (Fig. 3B). The introduction of non-conserved highly hydrophilic and charged arginine residue would most likely influence strong conformational change based on whether the mutated residue finally comes to lie on the surface or is accommodated inside the domain. Our choice of best possible rotamer during *in silico* mutagenesis suggests that the mutated arginine residue is most likely to be partially surface exposed with its charged side-chain, most likely resulting in a potential side-chain interaction with neighboring protein molecules which might accelerate the aggregation effect.

The LRR domain mutations R693P and R693W present an interesting scenario in whereby the same locus substitution shows different aggregation phenotypes (Fig. 3B). Unlike the R693W mutation, R693P does not result in an increased number of cells observed with large aggresome formations (Fig. 3A). This seems to be an anomaly since substitutions of Arg to Trp and to Pro are both almost equally non-conservative. However, the Trp substitution on position 693 is, unlike Pro, a non-conservative substitution with respect to hydrophobicity. Since the wild-type residue is located on the surface of the LRR domain, which is predominantly hydrophobic and only occasionally interrupted by large hydrophilic arginine residues, the addition of another highly hydrophobic residue, such as Trp, would contribute to the hydrophobic potential of this region and therefore potentiate its ability to aggregate. Also, since the residue runs down to a proximal region contributing to an oligomeric interface, as observed in our model (Fig. 3B; green arrow), the change in hydrophobic potential most likely influences the potential of this region to interact/aggregate. The Pro substitution, on the other hand, induces a structural knot and therefore results in a structurally misfolded protein with negative consequences on its function. However, regarding hydrophobicity, Pro would not be as much of a change as Trp and considering that the surface is not directly participating in the oligomeric interface, the Pro substitution would have little impact on aggregation/oligomerization.

The last missense variant K511R occurs on the interface of the LRR and NAD domain and actually shows a reduction in aggresome formation (Fig. 3C). This can be attributed to the fact that the substitution is semi-conservative and results only in a change in size. However, since the larger arginine side-chain is able to have more side-chain contacts than the lysine side-chain, it is very likely that the mutated arginine residues serve to further stabilize interactions between the LRR and NAD domain in the non-activated NLRP7 (Fig. 3B). This would provide additional rigidity to the structure, preventing any kind of conformational change required for either activation or aggresome formation.

Aggresome-based clearance of NLRP7: is it a pathological or a physiological regulatory mechanism in the cell?

Analysis of the effect of the three different HYDM1-causing missense mutations and the variant on the inter-domain interaction-related oligomerization of NLRP7 revealed no detectable influence in the yeast two-hybrid system (Supplementary data, Fig. S2). This is possibly due to the inactive state of the protein analyzed in the yeast system, while the impact of the mutations may only have an effect during or after activation of NLRP7. Accordingly and in contrast to yeast, two effects were observed in HEK293T cells with the two mutations L398R and R693W. Although the wild-type and the mutated protein did show the three different patterns of subcellular localization, the effect of juxtanuclear aggregation clearly increased in the presence of the two missense mutations L398R and R693W (Fig. 3C). Thus, co-immunoprecipitation of wild-type and each mutagenized NLRP7 construct with self-protein detected strong positive self-interactions for NLRP7wt, the rare variant K511R and the mild missense mutation R693P, while the two severe missense mutations L398R and R693W lost their interaction potential. This indicates that lesser intra-molecular interaction results in more aggregate formation. Hence, a balance between the two states exists in the wild-type molecules, while in severe mutants, it is shifted towards more aggregation.

Aggresomes are a general response of cells when the amount of accumulation and misfolded proteins prevails and the capacity of the proteasome is exceeded. Without ignoring the fact that overexpression of NLRP7 anyway leads to an overburdened proteasome, the LPS stimulation of PBMCs urges the native NLRP7 to co-localize with the MTOC, and disruption of the microtubule network after nocodazole treatment leads to a fragmentation of the polarized NLRP7 signal (Messaed *et al.*, 2011a). However, even with different transfection concentrations of NLRP7, we noticed that the two severe mutations, L398R and R693W, always show higher aggregate formation in comparison to the wild-type or the less severe mutations.

It is known that such cytoplasmic inclusions such as aggresomes are linked to the pathogenesis of many diseases, including Parkinson's disease and Huntington's disease. While both of these neurodegenerative disorders show intracellular protein aggregates, their origin and evolution are completely different. Currently, it is not known whether most of the diseases with protein aggregation are the cause or the consequence of some form of cellular dysfunction (Chanez-Cardenas and Vazquez-Contreras, 2012).

Recently, the role of protein misfolding and aggregation has become widely discussed in auto-inflammatory diseases (Park *et al.*, 2012). Several autosomal dominant mutations in *NLRP3* lead to different manifestations in the Cryopyrin-associated periodic syndrome (CAPS), such as the Muckle–Wells syndrome (MWS), familial cold auto-inflammatory syndrome (FCAS) or neonatal onset multi-system inflammatory disease (NOMID) (Ozkurede and Franchi, 2012). All CAPS disease-associated mutations are located in the NACHT domain of NLRP3 and are believed to enhance its oligomerization, inflammasome activation and subsequent processing of IL-1β (Agostini, 2004).

Accumulations of misfolded proteins can provoke processing of pro-inflammatory cytokines and abnormal intracellular signaling which lead to a gain of protein function in mechanisms that are related to the physiological role of the protein (Park *et al.*, 2012). This could involve the inflammasome-related pathway in innate immune cells or any other unknown NLRP7-related signaling pathway during gametogenesis, for instance, which are upstream signals important for the establishment of the maternal imprint. Clear links exist to IL-1β and reproduction, demonstrating that increased levels of IL-1β can induce ovulation in horse and rabbit but also lead to a developmental arrest of the embryo (Takehara *et al.*, 1994; Caillaud *et al.*, 2005).

Comparison of NLRP7 wild-type and three HYDM1-linked mutations (R693W, R693P and D657V) in the inflammasome reconstitution assay has already provided evidence that the mutations are more potent in activating the inflammasome and subsequent IL-1β secretion (Khare *et al.*, 2012). Keeping in mind that oligomerization/aggregation lies in the nature of NLRP7 and is indispensable for activation, we think that the process of physiologic oligomerization and pathologic aggregation follows a similar modus operandi. Hence, both processes might be similar and co-exist in a balanced manner, but in the presence of a particular missense mutation, the balance between oligomerization and aggregation may be shifted toward the latter.

In summary, our study presents the first model of NLRP7-specific inter-domain interactions, indicating NAD as the crucial interaction domain for oligomerization. Using *in silico* approaches, we also demonstrated the likely mechanism of NLRP7 activation. Moreover, our results serve as a basis for further analyses of HYDM1-causing mutations related to aggresome formation and suggest aggresome-based clearance as one of the new likely pathophysiological mechanisms for HYDM1-causing mutations in NLRP7.

Supplementary data

Supplementary data are available at http://molehr.oxfordjournals.org/.

Authors' roles

The authors were responsible for the following: experimental design (H.S., A.B. and O.E.-M.), data collection (H.S. and N.Z.), data analysis and figure production (H.S., A.B. and O.E.-M.), protein modeling (A.B.), and manuscript drafting and editing (H.S., A.B., C.M., J.O., R.S. and O.E.-M.).

Funding

This work was supported by internal funds of the Institute of Experimental Haematology and Transfusion Medicine of the University of Bonn and by an operating grant from the Canadian Institutes of Health Research (MOP 86546) to R.S.

Conflict of interest

None declared.

References

Agostini L. NALP3 forms an IL-1β-processing inflammasome with increased activity in Muckle-Wells autoinflammatory disorder. *Immunity* 2004; **20**:319–325.

Allen IC, Scull MA, Moore CB, Holl EK, McElvania-TeKippe E, Taxman DJ, Guthrie EH, Pickles RJ, Ting JP. The NLRP3 inflammasome mediates *in vivo* innate immunity to influenza A virus through recognition of viral RNA. *Immunity* 2009;**30**:556–565.

Bagola K, Sommer T. Protein quality control: on IPODs and other JUNQ. *Curr Biol* 2008;**18**:R1019–R1021.

Boyden ED, Dietrich WF. Nalp1b controls mouse macrophage susceptibility to anthrax lethal toxin. *Nat Genet* 2006;**38**:240–244.

Caillaud M, Duchamp G, Gerard N. *In vivo* effect of interleukin-1beta and interleukin-1RA on oocyte cytoplasmic maturation, ovulation, and early embryonic development in the mare. *Reprod Biol Endocrinol* 2005;**3**:26.

Carneiro LA, Magalhaes JG, Tattoli I, Philpott DJ, Travassos LH. Nod-like proteins in inflammation and disease. *J Pathol* 2008;**214**:136–148.

Chanez-Cardenas ME, Vazquez-Contreras E. The aggregation of huntingtin and alpha-synuclein. *J Biophys* 2012;**2012**:606172.

Danot O, Marquenet E, Vidal-Ingigliardi D, Richet E. Wheel of life, wheel of death: a mechanistic insight into signaling by STAND proteins. *Structure* 2009;**17**:172–182.

Davis IW, Leaver-Fay A, Chen VB, Block JN, Kapral GJ, Wang X, Murray LW, Arendall WB 3rd, Snoeyink J, Richardson JS *et al.* MolProbity: all-atom contacts and structure validation for proteins and nucleic acids. *Nucleic Acids Res* 2007;**35**:W375–W383.

Dias RP, Maher ER. Genes, assisted reproductive technology and trans-illumination. *Epigenomics* 2013;**5**:331–340.

Duncan JA, Bergstralh DT, Wang Y, Willingham SB, Ye Z, Zimmermann AG, Ting JP. Cryopyrin/NALP3 binds ATP/dATP, is an ATPase, and requires ATP binding to mediate inflammatory signaling. *Proc Natl Acad Sci USA* 2007;**104**:8041–8046.

El-Maarri O, Slim R. Familial hydatidiform molar pregnancy: the germline imprinting defect hypothesis? *Curr Top Microbiol Immunol* 2006;**301**:229–241.

El-Maarri O, Seoud M, Coullin P, Herbiniaux U, Oldenburg J, Rouleau G, Slim R. Maternal alleles acquiring paternal methylation patterns in biparental complete hydatidiform moles. *Hum Mol Genet* 2003;**12**:1405–1413.

Faustin B, Lartigue L, Bruey JM, Luciano F, Sergienko E, Bailly-Maitre B, Volkmann N, Hanein D, Rouiller I, Reed JC. Reconstituted NALP1 inflammasome reveals two-step mechanism of caspase-1 activation. *Mol Cell* 2007;**25**:713–724.

Fontalba A, Gutierrez O, Fernandez-Luna JL. NLRP2, an inhibitor of NF-kB pathway, is transcriptionally activated by NF-kB and exhibits a nonfunctional allelic variant. *J Immunol* 2007;**179**:8519–8524.

Hayward BE, De Vos M, Talati N, Abdollahi MR, Taylor GR, Meyer E, Williams D, Maher ER, Setna F, Nazir K *et al.* Genetic and epigenetic analysis of recurrent hydatidiform mole. *Hum Mutat* 2009;**30**:E629–E639.

Ishida T, Kinoshita K. PrDOS: prediction of disordered protein regions from amino acid sequence. *Nucleic Acids Res* 2007;**35**:W460–W464.

Johnston JA, Ward CL, Kopito RR. Aggresomes: a cellular response to misfolded proteins. *J Cell Biol* 1998;**143**:1883–1898.

Khare S, Dorfleutner A, Bryan NB, Yun C, Radian AD, de Almeida L, Rojanasakul Y, Stehlik C. An NLRP7-containing inflammasome mediates

recognition of microbial lipopeptides in human macrophages. *Immunity* 2012;**36**:464–476.

Kou YC, Shao L, Peng HH, Rosetta R, del Gaudio D, Wagner AF, Al-Hussaini TK, Van den Veyver IB. A recurrent intragenic genomic duplication, other novel mutations in NLRP7 and imprinting defects in recurrent biparental hydatidiform moles. *Mol Hum Reprod* 2008;**14**:33–40.

Krieger E, Koraimann G, Vriend G. Increasing the precision of comparative models with YASARA NOVA—a self-parameterizing force field. *Proteins* 2002;**47**:393–402.

Leipe DD, Koonin EV, Aravind L. STAND, a class of P-loop NTPases including animal and plant regulators of programmed cell death: multiple, complex domain architectures, unusual phyletic patterns, and evolution by horizontal gene transfer. *J Mol Biol* 2004;**343**:1–28.

Mariathasan S, Weiss DS, Newton K, McBride J, O'Rourke K, Roose-Girma M, Lee WP, Weinrauch Y, Monack DM, Dixit VM. Cryopyrin activates the inflammasome in response to toxins and ATP. *Nature* 2006;**440**:228–232.

Martinon F, Mayor A, Tschopp J. The inflammasomes: guardians of the body. *Annu Rev Immunol* 2009;**27**:229–265.

Messaed C, Akoury E, Djuric U, Zeng J, Saleh M, Gilbert L, Seoud M, Qureshi S, Slim R. NLRP7, a nucleotide oligomerization domain-like receptor protein, is required for normal cytokine secretion and co-localizes with Golgi and the microtubule-organizing center. *J Biol Chem* 2011a;**286**:43313–43323.

Messaed C, Chebaro W, Di Roberto RB, Rittore C, Cheung A, Arseneau J, Schneider A, Chen MF, Bernishke K, Surti U *et al*. NLRP7 in the spectrum of reproductive wastage: rare non-synonymous variants confer genetic susceptibility to recurrent reproductive wastage. *J Med Genet* 2011b; **48**:540–548.

Meyer E, Lim D, Pasha S, Tee LJ, Rahman F, Yates JR, Woods CG, Reik W, Maher ER. Germline mutation in NLRP2 (NALP2) in a familial imprinting disorder (Beckwith-Wiedemann Syndrome). *PLoS Genet* 2009;**5**:e1000423.

Murdoch S, Djuric U, Mazhar B, Seoud M, Khan R, Kuick R, Bagga R, Kircheisen R, Ao A, Ratti B *et al.* Mutations in NALP7 cause recurrent hydatidiform moles and reproductive wastage in humans. *Nat Genet* 2006;**38**:300–302.

Nguyen NM, Slim R. Genetics and Epigenetics of Recurrent Hydatidiform Moles: Basic Science and Genetic Counselling. *Curr Obstet Gynecol Rep* 2014;**3**:55–64.

Ozkurede VU, Franchi L. Immunology in clinic review series; focus on autoinflammatory diseases: role of inflammasomes in autoinflammatory syndromes. *Clin Exp Immunol* 2012;**167**:382–390.

Park H, Bourla AB, Kastner DL, Colbert RA, Siegel RM. Lighting the fires within: the cell biology of autoinflammatory diseases. *Nat Rev Immunol* 2012;**12**:570–580.

Peng H. NLRP2, a maternal effect gene required for early embryonic development in the mouse. *PLoS One* 2012;**7**:e303344.

Petrilli V, Dostert C, Muruve DA, Tschopp J. The inflammasome: a danger sensing complex triggering innate immunity. *Curr Opin Immunol* 2007; **19**:615–622.

Pettersen EF, Goddard TD, Huang CC, Couch GS, Greenblatt DM, Meng EC, Ferrin TE. UCSF Chimera—a visualization system for exploratory research and analysis. *J Comput Chem* 2004;**25**:1605–1612.

Pinheiro AS, Proell M, Eibl C, Page R, Schwarzenbacher R, Peti W. Three-dimensional structure of the NLRP7 pyrin domain: insight into pyrin-pyrin-mediated effector domain signaling in innate immunity. *J Biol Chem* 2010;**285**:27402–27410.

Proell M, Riedl SJ, Fritz JH, Rojas AM, Schwarzenbacher R. The Nod-like receptor (NLR) family: a tale of similarities and differences. *PLoS One* 2008;**3**:e2119.

Reubold TF, Wohlgemuth S, Eschenburg S. A new model for the transition of APAF-1 from inactive monomer to caspase-activating apoptosome. *J Biol Chem* 2009;**284**:32717–32724.

Slim R, Wallace EP. NLRP7 and the genetics of hydatidiform moles: recent advances and new challenges. *Front Immunol* 2013;**4**:242.

Takehara Y, Dharmarajan AM, Kaufman G, Wallach EE. Effect of interleukin-1 beta on ovulation in the *in vitro* perfused rabbit ovary. *Endocrinology* 1994; **134**:1788–1793.

Tian X, Pascal G, Monget P. Evolution and functional divergence of NLRP genes in mammalian reproductive systems. *BMC Evol Biol* 2009;**9**:202.

Tong Z-B, Gold L, Pfeifer KE, Dorward H, Lee E, Bondy CA, Dean J, Nelson LM. Mater, a maternal effect gene required for early embryonic development in mice. *Nat Genet* 2000;**26**:267–268.

Van Durme J, Delgado J, Stricher F, Serrano L, Schymkowitz J, Rousseau F. A graphical interface for the FoldX forcefield. *Bioinformatics* 2011; **27**:1711–1712.

Yang J, Roy A, Zhang Y. Protein-ligand binding site recognition using complementary binding-specific substructure comparison and sequence profile alignment. *Bioinformatics* 2013;**29**:2588–2595.

Yuan S, Topf M, Reubold TF, Eschenburg S, Akey CW. Changes in Apaf-1 conformation that drive apoptosome assembly. *Biochemistry* 2013; **52**:2319–2327.

Zhang Y. I-TASSER server for protein 3D structure prediction. *BMC Bioinformatics* 2008;**9**:40.